Electrochemistry Communications 107 (2019) 106510

Contents lists available at ScienceDirect

Electrochemistry Communications

journal homepage: www.elsevier.com/locate/elecom

Short communication

Metal–metal oxide nanostructure supported on graphene oxide as a multifunctional electro-catalyst for simultaneous detection of hydrazine and hydroxylamine

Maria Sarno[a,b,*], Eleonora Ponticorvo[b]

[a] Department of Industrial Engineering, University of Salerno, Via Giovanni Paolo II, 132, 84084 Fisciano, SA, Italy
[b] NANO_MATES, Research Centre for Nanomaterials and Nanotechnology at the University of Salerno, University of Salerno, Via Giovanni Paolo II, 132, 84084 Fisciano, SA, Italy

ARTICLE INFO

Keywords:
Ir and Ru active phases
New synthesis protocol
Hydrazine
Hydroxylamine
Low detection limit

ABSTRACT

A ruthenium/iridium/iridium oxide nanohybrid supported on graphene oxide (RuIrOx_GO) was prepared via a new protocol. The activity of the nanohybrid towards the simultaneous detection of hydrazine (HY) and hydroxylamine (HA) was evaluated in phosphate-buffered saline solution (pH 7.0). Differential pulse voltammetry was used for the measurements, with a pulse amplitude of 50 mV and a scan rate of 0.04 V s^{-1}. Using the modified electrode, the oxidation peak potentials for HY and HA can be easily distinguished, with a large peak separation of 0.36 V. Very low LOD values of 2.1 μM and 1.6 μM were found for HY and HA, respectively. The selectivity of the electrode and its stability were also studied The tolerance limits in the presence of different interfering compounds were evaluated. After five weeks, a deviation from the expected results of ~2% was observed for both HA and HY determinations.

1. Introduction

Detection of the class of natural organic pollutants containing nitrogen is a topic of significant importance in the context of environmental control. Among these, hydrazine (HY) and hydroxylamine (HA) are often present at the same time. In particular, hydrazine (HY) is widely used as a reducing agent in fuel cells, an intermediate in pesticide production, a scavenger, as a regulator of plant growth, a catalyst, an anti-corrosion agent, and an anti-oxidant [1]. It is toxic [2] and an object of pharmacological attention. Hydroxylamine (HA), which is also an intermediate in the nitrogen cycle, is widely used in industry as a reducing agent [3] and is also used in anti-cancer treatments [4]. This compound is toxic for flora, fauna, and humans, even at low doses [5].

A range of different methods (potentiometry, spectrophotometry, mass spectrometry, etc.) can be used for determination of HY and HA. Because of the polarity of these molecules, their easy oxidation, absence of chromophores and molecular weight, all these methods have advantages and limitations [6,7]. Although chromatographic methods are a good analytical alternative, they involve complex and time-consuming procedures, and are subject to interference due to reactions occurring within the system being analysed [8].

Electrochemical approaches provide a valid alternative, due to their sensitivity, reliability, and ease of use. In terms of electrochemical determination of HA and HY, a number of papers have been published on hydrazine [9–13] and hydroxylamine [14–19] detection. In general, high overpotentials are required for hydrazine and hydroxylamine oxidation at bare surfaces, while overlapping responses can occur during simultaneous detection, making determination impossible [20–23]. Therefore, there is a need to fabricate simple, fast, selective, stable, and sensitive systems based on modified surfaces capable of the simultaneous determination of these two species.

A lot of investigative effort has recently been devoted to the intriguing electrochemical properties of nanoparticles (NPs) [24–26]. Metal and metal oxide NPs have received attention due to their particular characteristics, such as their conductivity and their excellent electrocatalytic and electroanalytical properties, mainly due to their nano size [24,27]. In particular, electron transfer at the electrode/analyte interface is favored in the presence of NPs [27]. A considerable number of NPs, including metallic NPs [24,28] and oxide NPs [29–31], have been tested for detection of different species. Among those studied, ruthenium and its derivatives have shown considerable ability as electrode modifiers [9,32].

The simultaneous detection of HY and HA could be achieved through the development of a precisely controlled (e.g., size, chemistry

* Corresponding author at: Department of Industrial Engineering, University of Salerno, Via Giovanni Paolo II, 132, 84084 Fisciano, SA, Italy.
E-mail address: msarno@unisa.it (M. Sarno).

https://doi.org/10.1016/j.elecom.2019.106510
Received 14 June 2019; Received in revised form 1 August 2019; Accepted 2 August 2019
Available online 06 September 2019
1388-2481/ © 2019 Published by Elsevier B.V. This is an open access article under the CC BY-NC-ND license (http://creativecommons.org/licenses/BY-NC-ND/4.0/).

and shape) metal/metal oxide electrocatalyst. In other contexts, successful preparation of catalytically active Au/Au_2O_3 [33], Ru/RuO_2 [34], Pd/PdO [35] and Pt/PtO_2 [26] has been reported, demonstrating that a metal/metal oxide interface can improve the electrocatalytic activity of the active metal catalyst.

The combination of iridium and ruthenium-based oxidation catalysts represents one possible solution. Indeed, apart from Ru oxide electrode sensors [9,32], Ir and Ru oxides have been found to be very active anode materials [36–39] with a low overpotential for the oxygen evolution reaction (OER) [39] and iridium oxide also demonstrating long-term stability [40]. Moreover, the combination of Ir and Al_2O_3 constitutes a well-known commercial hydrazine activator, even at 293 K [41]. This robust catalyst, stable under the overpressure of repeated ignitions and characterized by great hardness, is used in the ignition of rocket motors using HA fuel.

Here, for the first time, based on previous experience and studies, we introduce an innovative protocol, designed to be 'green' and operate under mild conditions, for the preparation of a ruthenium/iridium-iridium oxide supported nanocomposite which can be used as an electrocatalyst, for HA and HY oxidation and their simultaneous detection. In particular, during the synthesis, which is performed at low temperature in water and in the absence of surfactants, the functional groups, i.e., the –OH groups of graphene oxide, themselves act as reducing agents and anchoring points for the formation of stable nanoparticles dispersed over a robust electrode. This study demonstrates that the modified electrode is capable of distinguishing these two analytes with two well-separated voltage peaks. The modified electrode exhibits a low limit of detection (LOD) over repeated cycles of usage.

2. Materials and methods

2.1. Preparation of the nanohybrid

The procedure for fabrication of the nanosensor is shown in Fig. 1. $RuCl_3$·xH2O (0.1 mmol) and $IrCl_3$ (0.125 mmol) were dissolved in distilled water (200 mL) at 20 °C, and NH_3·H_2O (4.0 M) was then added dropwise to reach pH = 10. Graphene oxide (GO) (100 mg) was then gradually added to the solution with magnetic stirring. The resulting mixture was heated to 60 °C and stirred for 1 h. The pH was maintained at 10 throughout this procedure. Subsequently, the final product was obtained after centrifugation, drying at 80 °C overnight and calcination at 150 °C for 2 h.

2.2. Characterization techniques

A number of methods were used to characterize the materials. An FEI Tecnai electron microscope, equipped with an EDX probe, was used to obtain transmission electron microscopy (TEM) images. A Phenom electron microscope was used for scanning electron microscopy (SEM) characterization. X-ray diffraction patterns were acquired by means of a Bruker D8 X-ray diffractometer. A micro- Raman spectrometer (Renishaw inVia, UK, 514 nm excitation wavelength) was used to obtain Raman spectra. N_2 adsorption–desorption (Kelvin 1042 V3.12, COSTECH Instruments) at 77 K makes it possible to determine the surface area, after 250 °C for 3 h pretreatment in He. A PHI-550 Multitechnique spectrometer was used for XPS measurements.

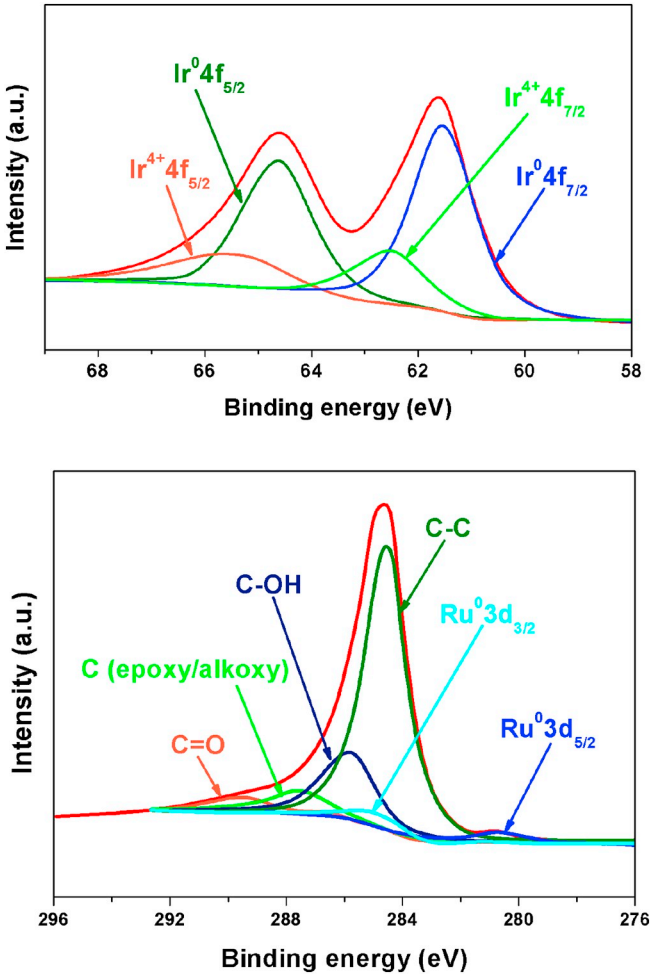

Fig. 2. XPS analysis of RuIrOx_GO nanohybrid.

2.3. Electrochemical measurements

A potentiostat/galvanostat (PGSTAT302N Autolab Instruments Metrohm) was employed for the electrochemical measurements, using screen-printed platinum-based electrodes (SPEs). The electrochemical

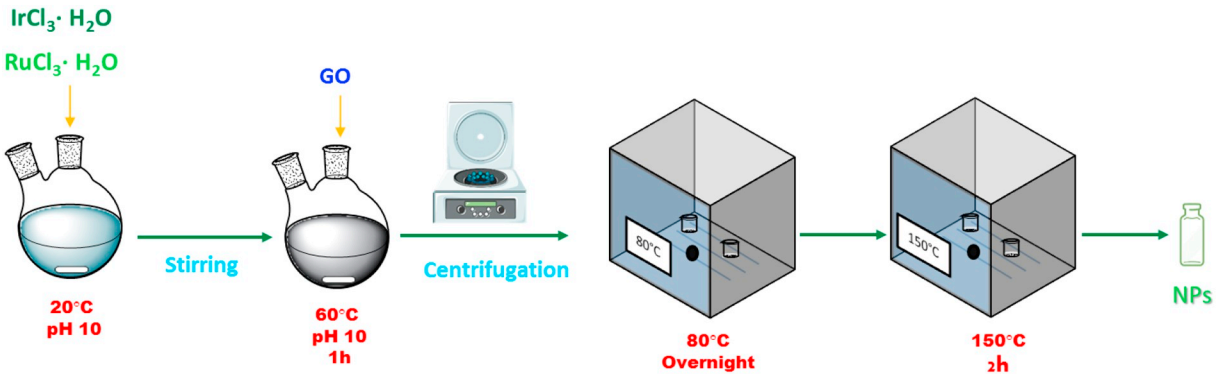

Fig. 1. Synthesis of IrRuOx_GO nanohybrid.

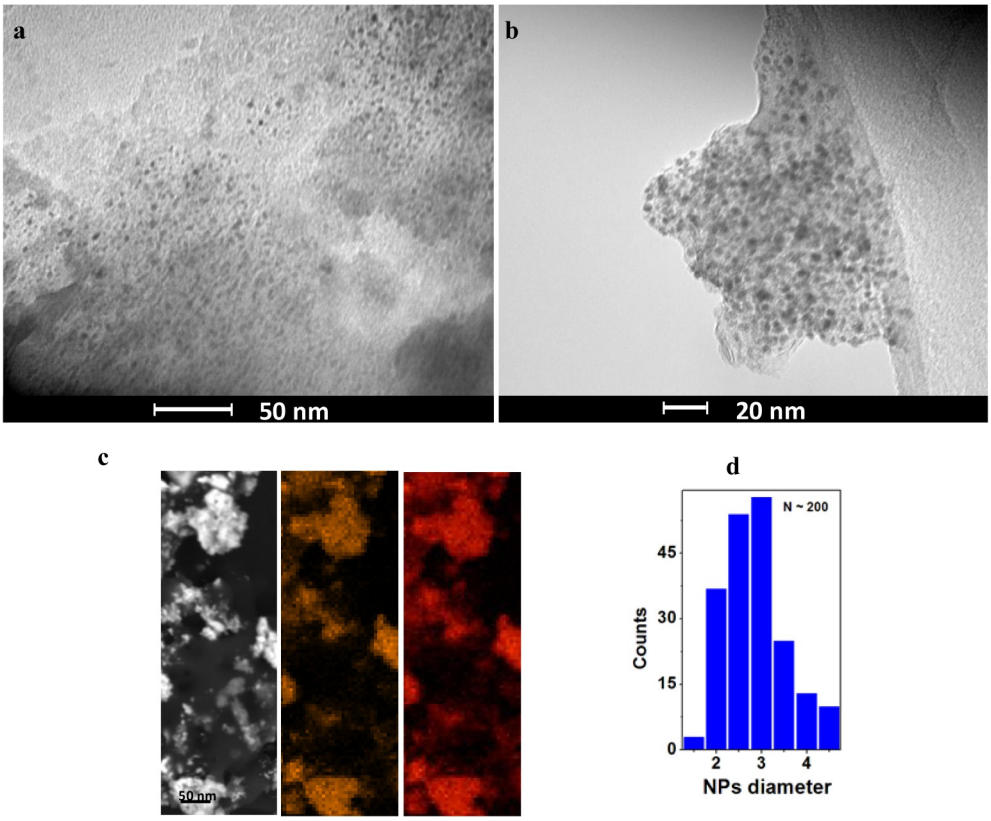

Fig. 3. (a, b) TEM images of RuIrOx_GO nanohybrid at different magnifications; (c) FESEM image of RuIrOx_GO nanohybrid and EDX maps of ruthenium (orange) and iridium (red); (d) size distribution histogram. (For interpretation of the references to color in this figure legend, the reader is referred to the web version of this article.)

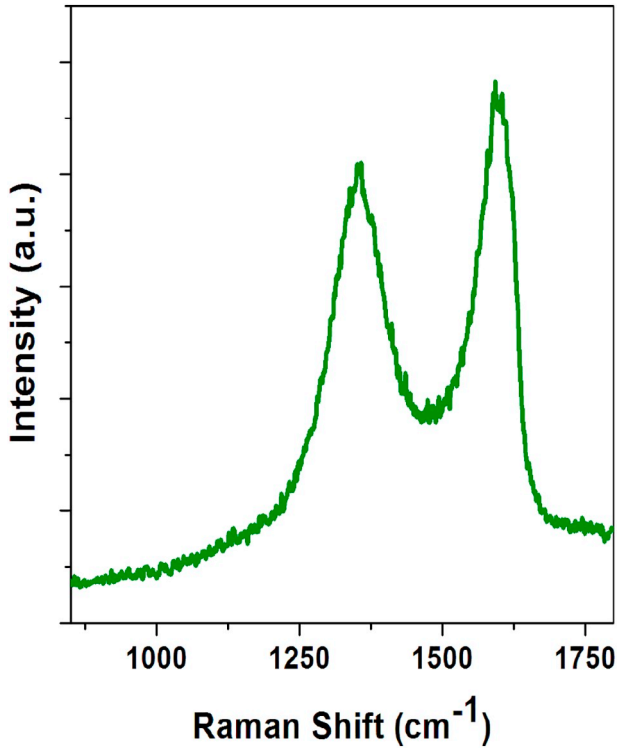

Fig. 4. Raman spectrum of RuIrOx_GO nanohybrid in the range 850–1800 cm^{-1}.

performance of the sensor was evaluated in PBS (phosphate buffer solution) at pH 7.0. A modulation amplitude of 50 mV was used for DPV (differential pulse voltammetry).

2.4. Electrochemical sensor preparation

A homogeneous ink was prepared by mixing 4 mg of the catalyst with 5 wt% Nafion solution (80 µL). The slurry/dispersions were dropped onto the SPEs to produce modified electrodes [42].

3. Results and discussion

3.1. Characterization of RuIrOx_GO

Surface analysis of RuIrOx_GO was performed using XPS, see Fig. 2. The Ir 4f XPS spectrum can be fitted by two pairs of curves, indicating the simultaneous presence of metallic and oxidized phases. Metallic Ir (0) is responsible for the 61.56 and 64.61 eV peaks. On the other hand, the peaks at 62.54 and 65.60 eV are due to the Ir(IV) oxidized phase. The electronic state of Ru is partially overlapped with the C1s peak. The binding energy of Ru $3d_{5/2}$ is at 280.69 eV, slightly shifted (less than 0.5 eV) with respect to metallic Ru, because of the electron transfer between Ru and O_2 in graphene oxide. Four peaks can be used to deconvolute the C1s spectrum of graphene oxide: at 284.54, 285.80, 287.54 and 289.69 eV, likely due to carbon–carbon, carbon–OH, epoxy/alkoxy carbon and carbonyl groups, respectively.

The TEM images in Fig. 3a–b reveal the formation of NPs dispersed on GO, preventing aggregation. The NPs appear to be anchored to the substrate even after the ultrasonication used for TEM preparation. The SEM images are shown in Fig. 3c. The EDX maps provide both topographical and quantitative information about the nanoparticles. The Ir and Ru maps are superimposable, indicating a homogeneous distribution. The distribution of NP sizes is shown in Fig. 3d. The average diameter was 2.8 nm with a standard deviation of 1.8 nm.

The Raman spectrum of the nanohybrid is shown in Fig. 4. This displays the two characteristic Raman bands of nanocarbons, centred at 1351 and 1595 cm^{-1}, which can be assigned to the D and G bands, respectively [43]. No peaks from Ir oxides were detected, indicating the

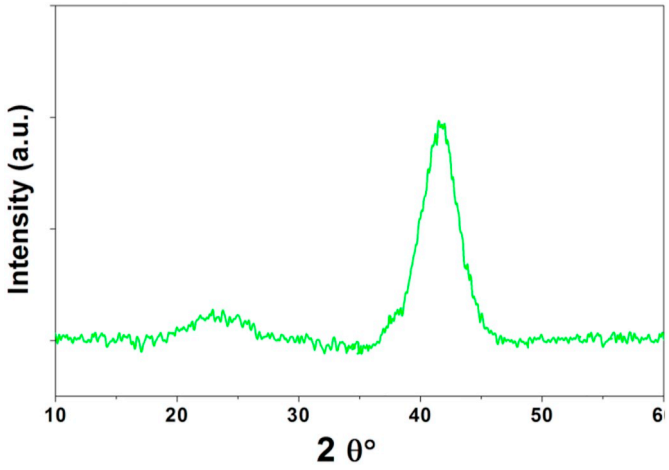

Fig. 5. XRD pattern of RuIrOx_GO nanohybrid.

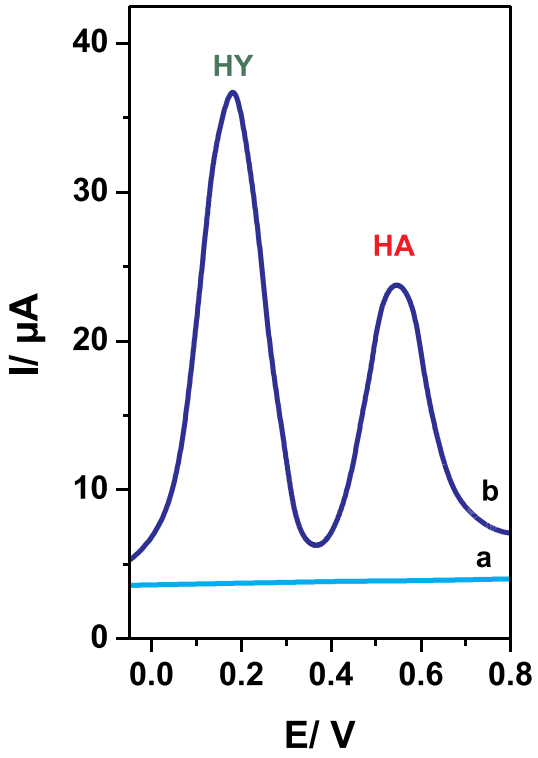

Fig. 6. DPV of RuIrOx_GO nanohybrid in PBS, without (cyan) and with (blue) hydrazine (0.3 mM) and hydroxylamine (0.5 mM), recorded at a scan rate of 0.04 V s^{-1}. (For interpretation of the references to color in this figure legend, the reader is referred to the web version of this article.)

small size of Ir oxide inclusions.

Fig. 5 shows the XRD spectrum of the prepared nanosensor. The peak at 42.7° is due to a Ru– Ir alloy hcp structure [44,45], in line with the phase equilibrium of Ru and Ir in alloy form [46]. It is worth noting that this peak is shifted to a lower angle than the corresponding peak of Ru(101), which is typically at 43.6° [44], indicating the formation of a Ru-Ir alloy. The broad peak at about 2θ = 26.10° corresponds to the typical 002 planes of graphite and indicates that reduction of GO occurred during sample preparation.

The BET surface area for RuIrOx_GO obtained from N_2 adsorption–desorption analysis is equal to 93.14 m^2/g. The distribution is a multimodal, BJH (Barrett – Joyner – Halenda) pore distribution, centered at 2.8, 5.9, 9.4 and 32.5 nm, indicating a network of larger and

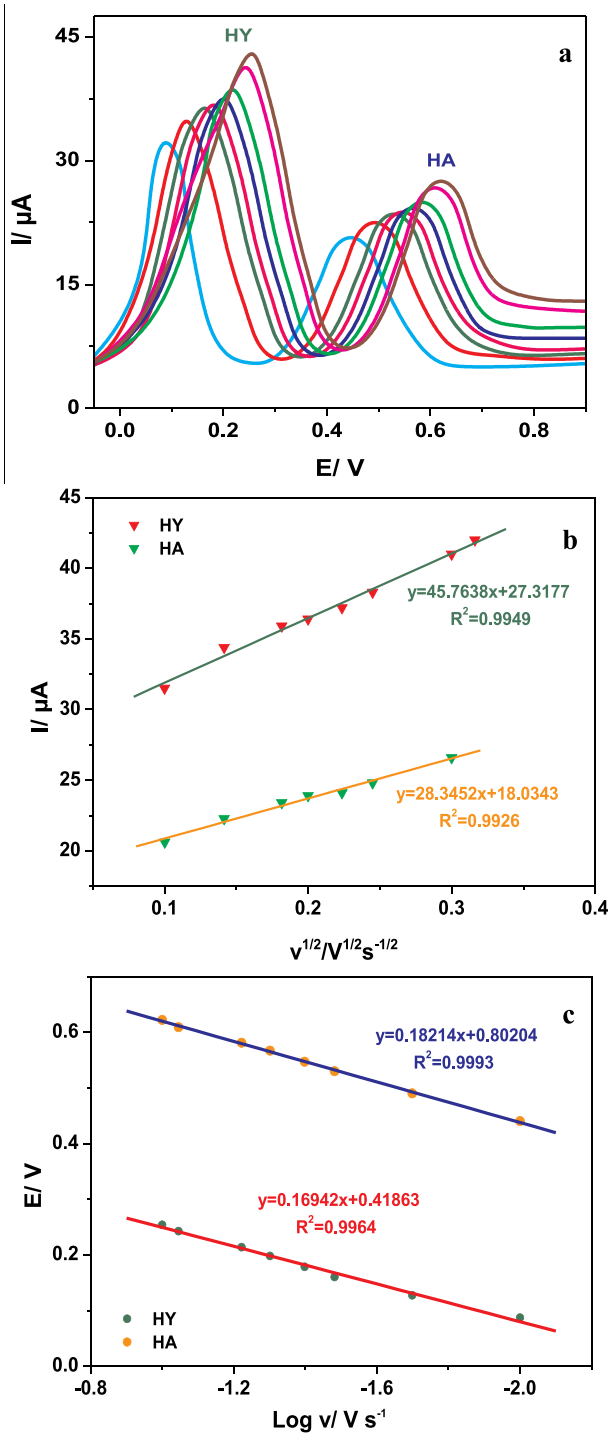

Fig. 7. (a) DPV of RuIrOx_GO nanohybrid in PBS at various scan rates, 0.01–0.1 V s^{-1}; (b) I vs. $v^{1/2}$; (c) E vs. Log v.

smaller pores enabling electrode wettability and exposing surface nanoparticles.

3.2. Electrochemical RuIrOx_GO sensor

The profiles shown in cyan and blue in Fig. 6 illustrate the behavior of RuIrOx_GO during scans in the absence of HY and HA, and in the presence of HY (0.3 mM) and HA (0.5 mM) in PBS at pH 7.0, respectively. The measurements were carried out by DPV (scan rate 0.04 V s^{-1}). Two clear oxidation peaks with a large peak separation

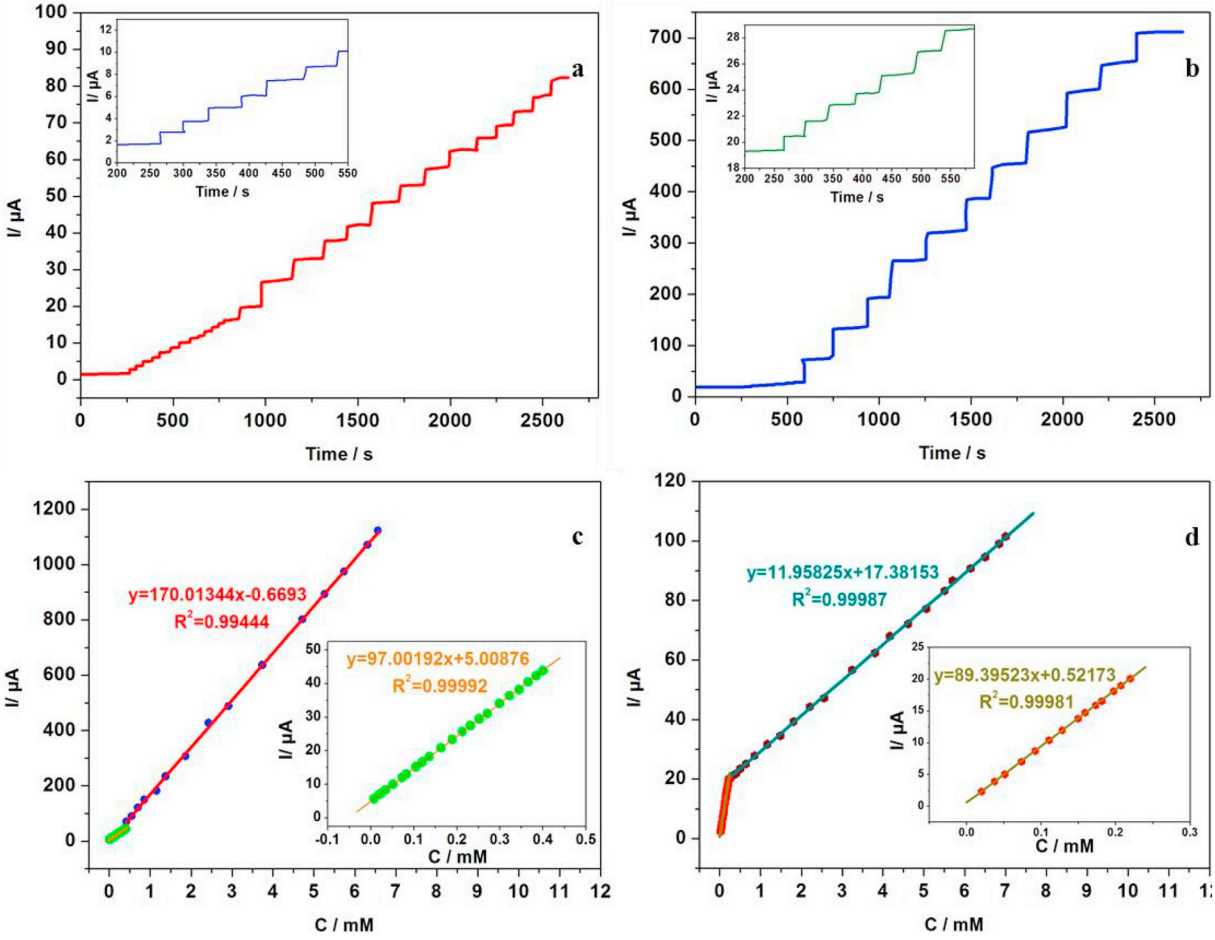

Fig. 8. Amperometric responses of the RuIrOx_GO nanohybrid after successive addition of (a) hydrazine at 0.18 V and (b) hydroxylamine at 0.54 V in a stirred PBS, at pH 7.0. Calibration plots of RuIrOx_GO at different concentrations of (c) hydrazine (from 0.01 mM to 6.5 mM) and (d) hydroxylamine (from 0.02 mM to 7.0 mM).

Table 1
Interference analysis for the determination of hydrazine and hydroxylamine in PBS, at pH 7.0.

Species	Tolerance limit (M)
NO_3^-, Na^+, K^+, F^-, Br^-, S^{2-}, CO_3^{2-}, Ni^{2+}, PO_4^{3-}, NO_2^-, Ca^{2+}, I^-, Mg^{2+}, CH_3COO^-, NH_4^+, Cl^-, Ba^{2+}, Zn^{2+}, Fe^{2+}, Fe^{3+}	$0.8 * 10^{-1}$
Ethanol, glucose, hydrogen peroxide, urea, tartaric acid	$4.6 * 10^{-3}$

(0.36 V) can be observed. The curves exhibit high current densities and low oxidation voltages of 0.18 and 0.54 V (vs. Ag/AgCl) for HY and HA, respectively. Thus we can conclude that when RuIrOx_GO is used as a working electrode, good separation of the HY and HA anodic peaks is achieved.

DPVs of RuIrOx_GO were obtained at different scan rates from 0.01 to 0.1 V s^{-1} (Fig. 7a).

The anodic peak currents show a linear correlation with the scan rate $v^{1/2}$ (Fig. 7b), indicating that the process is controlled by diffusion phenomena [47]. Moreover, as the scan rate increases, the oxidation voltages for hydrazine and hydroxylamine shift to more positive values, suggesting that the reactions of HY and HA on the RuIrOx_GO electrode are irreversible [48–50]. The behavior of the HY and HA oxidation peak potentials with increasing scan rate (v) is shown in Fig. 7c. The Tafel slope b is equal to ($2.303RT/\alpha nF$) [49], where α is the transfer coefficient and n the number of electrons transferred. The calculated values of αn are 0.694 and 0.650 for HY and HA, respectively. Assuming that one electron transfer is the rate-determining step (n = 1), the transfer coefficient α assumes the values of 0.69 and 0.65 for HY and HA, respectively, in agreement with the typical range 0.3–0.7 [51,52].

Fig. 8a and b show the amperometric responses of RuIrOx_GO during a series of separate additions of HY at 0.18 V and HA at 0.54 V, respectively, in stirred PBS at pH 7.0.

The amperometric response is a more effective method for the determination of low concentrations of analytes. The sensor displays a rapid amperometric response, reaching a new steady-state condition within ~4 s. The current response calibration plots for hydrazine and hydroxylamine are shown in Fig. 8c and d. The current response has a linear correlation with concentrations from the very low value of 0.01 mM to 0.4 mM and from 0.4 mM to 6.5 mM, for HY. Over the wide ranges [1,23,53,54] of 0.02 mM to 0.2 mM and 0.2 mM to 7.0 mM, linear relationships were also obtained for hydrazine. Very low LOD values of 2.1 μM and 1.6 μM (S/N = 3) are achieved for hydrazine and hydroxylamine, respectively, with R^2 close to 1 in both cases.

Apart from the novelty of the surface modifier and the preparation method used, our LODs have been obtained over larger ranges than in refs. 1, 23, 53, 54, and with a higher voltage difference between the two peaks of detection than in refs 1 and 53.

3.3. Interference and stability analyses

When trying to determine the concentration of HY and HA, a further key issue is the effect of the presence of potential interfering ions and electro-active species containing nitrogen, which are typically present

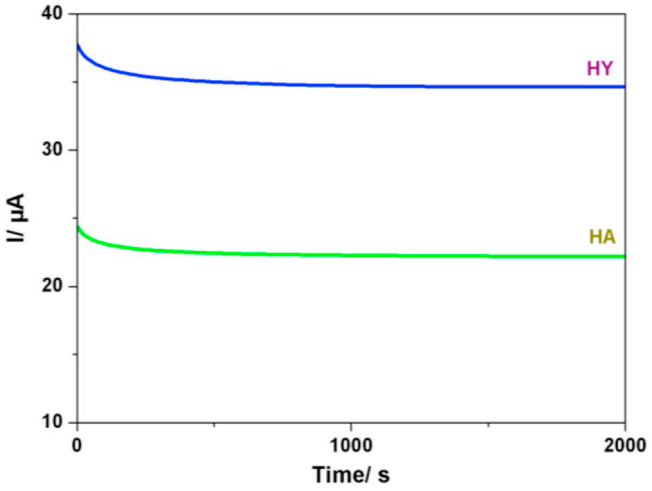

Fig. 9. Long-term current–time curves of RuIrOx_GO nanohybrid for HY and HA detection.

in natural water and industrial waste-waters, as well as being produced by the nitrogen cycle.

The effects of different potential interfering compounds were evaluated using 0.4 mM of HY and HA in PBS at pH 7.0. The tolerance limits are shown in Table 1. These were assessed at the maximum concentration, which caused about ± 5% of determination error.

The stability of the RuIrOx_GO-modified SPEs was also evaluated. The electrodes were stored in PBS solution at room temperature for 5 weeks and washed before each use. A deviation from the expected results of ~2% was observed for both HA and HY. To evaluate the reproducibility of the RuIrOx_GO-based sensor, three electrodes made under the same experimental conditions were tested by DPV. A relative standard deviation of 1.8% was obtained, demonstrating appropriate sensor reproducibility.

Fig. 9 shows the long-term current–time stability of RuIrOx_GO at 0.18 and 0.54 V (vs. Ag/AgCl) for HY and HA, respectively. The experiments were performed for 2000 s in a PBS buffer solution containing HY (0.3 mM) and HA (0.5 mM). A ~94% retention of the initial response was observed for both HY and HA.

4. Conclusions

A ruthenium/iridium-iridium oxide supported nanocomposite was generated through an easy, scalable new protocol under mild conditions. TEM analysis confirmed the formation of nanoparticles, with an average diameter of 2.8 nm, dispersed on GO preventing aggregation. Ir and Ru EDX maps were superimposable, indicating a homogeneous distribution of metals in the nanoparticles. The XPS and XRD analyses show the formation of a Ru-Ir alloy, the presence of IrOx and the reduction of GO during the sample preparation. RuIrOx_GO showed excellent behavior as a HA and HY sensor: high-value oxidation peak separation (0.36 V), high current intensities, very wide linear ranges of detection and low detection limits (2.1 and 1.6 µM for HY and HA, respectively). These results are likely due to: the favorable porous structure of the electrode; its large surface area; the high conductivity of the GO network; and the promoter role of the oxides, which favor accumulation of metal charges and thus electron exchange between the analytes and the electrode. Moreover, the selectivity of the electrode was evaluated in the presence of several potentially interfering compounds, finding no significant interference.

References

[1] F. Tahernejad-Javazmi, M. Shabani-Nooshabadi, H. Karimi-Maleh, H. Naeimi, Square wave voltammetric determination of hydrazine and 4-chlorophenol as two important water pollutants using nanostructure-amplified sensor, Res. Chem. Intermed. 44 (2018) 5389–5401.
[2] Y. Wang, X. Yang, J. Bai, X. Jiang, G. Fan, High sensitivity hydrogen peroxide and hydrazine sensor based on silver nanocubes with rich {100} facets as an enhanced electrochemical sensing platform, Biosens. Bioelectron. 43 (2013) 180–185.
[3] X.P. Cui, L. Hong, X.Q. Lin, Electrocatalytic oxidation of hydroxylamine on glassy carbon electrodes modified by hybrid copper–cobalt hexacyanoferrate films, Anal. Sci. 18 (2002) 543–547.
[4] G. Sosnovsky, P. Bell, In the search for new anticancer drugs. 29. A study on the correlation of lipophilicities, ionization constants and anticancer activities of aminoxyl labeled tepa congeners, Life Sci. 62 (1998) 639–648.
[5] T. Hofman, H. Lees, The biochemistry of the nitrifying organisms. 4. The respiration and intermediary metabolism of *Nitrosomonas*, Biochem. J. 54 (1953) 579–583.
[6] B.R. Sant, Oxidation of hydroxylamine by ferricyanide in presence of zinc sulfate: a rapid method for estimating hydroxylamine and hydrazine in a mixture, Anal. Chim. Acta 20 (1959) 371–375.
[7] M.D. Morris, J.J. Lingane, The simultaneous determination of hydrazine and hydroxylamine: an analytical application of chronopotentiometry, J. Electroanal. Chem. 8 (1964) 85–92.
[8] A.D. Smolenkov, O.A. Shpigun, Direct liquid chromatographic determination of hydrazines: a review, Talanta 102 (2012) 93–100.
[9] A. Abbaspour, M. Shamsipur, A. Siroueinejad, R. Kia, P.R. Raithby, Renewable-surface sol–gel derived carbon ceramic-modified electrode fabricated by a newly synthesized polypyridil and phosphine Ru (II) complex and its application as an amperometric sensor for hydrazine, Electrochim. Acta 54 (2009) 2916–2923.
[10] S.M. Golabi, H.R. Zare, Electrocatalytic oxidation of hydrazine at a chlorogenic acid (CGA) modified glassy carbon electrode, J. Electroanal. Chem. 465 (1999) 168–176.
[11] I.G. Casella, M.R. Guascito, A.M. Salvi, E. Desimoni, Catalytic oxidation and flow detection of hydrazine compounds at a nafion/ruthenium(III) chemically modified electrode, Anal. Chim. Acta 354 (1997) 333–341.
[12] S. Babanova, U. Martinez, K. Artyushkova, K. Asazawa, H. Tanaka, P. Atanassov, Hydrazine sensor for quantitative determination of high hydrazine concentrations for direct hydrazine fuel cell vehicle applications, J. Electrochem. Soc. 161 (2014) H79–H85.
[13] A. Abbaspour, A. Khajehzadeh, A. Ghaffarinejad, Electrocatalytic oxidation and determination of hydrazine on nickel hexacyanoferrate nanoparticles-modified carbon ceramic electrode, J. Electroanal. Chem. 631 (2009) 52–57.
[14] R. Sadeghi, H. Karimi-Maleh, M.A. Khalilzadeh, H. Beitollahi, Z. Ranjbarha, M.B.P. Zanousi, A new strategy for determination of hydroxylamine and phenol in water and waste water samples using modified nanosensor, Environ. Sci. Pollut. Res. 20 (2013) 6584–6593.
[15] M.P.N. Bui, X.H. Pham, K.N. Han, C.A. Li, E.K. Lee, H.J. Chang, G.H. Seong, Electrochemical sensing of hydroxylamine by gold nanoparticles on single-walled carbon nanotube films, Electrochem. Commun. 12 (2010) 250–253.
[16] Y. Geng, E. Ko, V.K. Tran, W.S. Chung, C.H. Park, M.K. Kim, G.H. Jin, G.H. Seong, Electrochemical detection of hydroxylamine via Au-Pt alloy nanoparticle- modified single-walled carbon nanotube electrodes, Anal. Sci. 33 (2017) 993–998.
[17] M.M. Foroughi, H. Beitollahi, S. Tajik, M. Hamzavi, H. Parvan, Hydroxylamine electrochemical sensor based on a modified carbon nanotube paste electrode: application to determination of hydroxylamine in water samples, Int. J. Electrochem. Sci. 9 (2014) 2955–2965.
[18] Y. Wang, L. Wang, H. Chen, X. Hu, S. Ma, Fabrication of highly sensitive and stable hydroxylamine electrochemical sensor based on gold nanoparticles and metal – metalloporphyrin framework modified electrode, ACS Appl. Mater. Interfaces 8 (2016) 18173–18181.
[19] A.D. Goolsby, D.T. Sawyer, The electrochemical oxidation of hydroxylamine at platinum and gold electrodes in dimethylsulfoxide, J. Electroanal. Chem. Interfacial Electrochem. 19 (1968) 405–411.
[20] S. Rostami, S.N. Azizi, S. Ghasemi, Simultaneous electrochemical determination of hydrazine and hydroxylamine by CuO doped in ZSM-5 nanoparticles as a new amperometric sensor, New J. Chem. 41 (2017) 13712–13723.
[21] E. Lee, D. Kim, J.M. You, S.K. Kim, M. Yun, S. Jeon, Electrocatalytic oxidation of hydrazine and hydroxylamine by graphene oxide-Pd nanoparticle-modified glassy carbon electrode, J. Nanosci. Nanotechnol. 12 (2012) 8886–8892.
[22] J. Li, X. Lin, Electrocatalytic oxidation of hydrazine and hydroxylamine at gold nanoparticle—polypyrrole nanowire modified glassy carbon electrode, Sens. Actuators B Chem. 126 (2007) 527–535.
[23] M. Mazloum-Ardakani, A. Khoshroo, L. Hosseinzadeh, Simultaneous determination of hydrazine and hydroxylamine based on fullerene-functionalized carbon nanotubes/ionic liquid nanocomposite, Sens. Actuators B Chem. 214 (2015) 132–137.
[24] S. Liu, J. Yu, H. Ju, Renewable phenol biosensor based on a tyrosinase-colloidal old modified carbon paste electrode, J. Electroanal. Chem. 540 (2003) 61–67.
[25] M. Sarno, E. Ponticorvo, Effect of the amount of nickel sulphide, molybdenum disulphide and carbon nanosupport on a Tafel slope and overpotential optimization, Nanotechnology 28 (2017) 214003.
[26] M. Sarno, E. Ponticorvo, Much enhanced electrocatalysis of Pt/PtO_2 and low platinum loading Pt/PtO2-Fe_3O_4 dumbbell nanoparticles, Int. J. Hydrog. Energy 42 (2017) 23631–23638.
[27] R. Narayanan, M.A. El-Sayed, Effect of catalytic activity on the metallic nanoparticle size distribution: electron-transfer reaction between $Fe(CN)_6$ and thiosulfate ions catalyzed by PVP – platinum nanoparticles, J. Phys. Chem. B 107 (2003) 12416–12424.
[28] Y. Wu, J. Zheng, Z. Li, Y. Zhao, Y. Zhang, A novel reagentless amperometric immunosensor based on gold nanoparticles/TMB/Nafion-modified electrode, Biosens. Bioelectron. 24 (2009) 1389–1393.
[29] A. Salimi, E. Sharifi, A. Noorbakhsh, S. Soltanian, Direct electrochemistry and

electrocatalytic activity of catalase immobilized onto electrodeposited nano-scale islands of nickel oxide, Biophys. Chem. 125 (2007) 540–548.
[30] G. Zhao, J.J. Feng, J.J. Xu, H.Y. Chen, Direct electrochemistry and electrocatalysis of heme proteins immobilized on self-assembled ZrO_2 film, Electrochem. Commun. 7 (2005) 724–729.
[31] E. Topoglidis, C.J. Campbell, A.E.G. Cass, J.R. Durrant, Nitric oxide biosensors based on the immobilization of hemoglobin on mesoporous titania electrodes, Electroanalysis 18 (2006) 882–887.
[32] L. Cheng, G.E. Pacey, J.A. Cox, Carbon electrodes modified with ruthenium metallodendrimer multilayers for the mediated oxidation of methionine and insulin at physiological pH, Anal. Chem. 73 (2001) 5607–5610.
[33] X. He, H.M. Yang, Au nanoparticles assembled on palygorskite: enhanced catalytic property and $Au-Au_2O_3$ coexistence, J. Mol. Catal. A Chem. 379 (2013) 219–224.
[34] Y.H. Li, Q. Zhan, N.W. Zhan, L.H. Zhu, J.B. Zhen, B.H. Chen, $Ru-RuO_2$/C as an efficient catalyst for the sodium borohydride hydrolysis to hydrogen, Int. J. Hydrog. Energy 38 (2013) 13360–13367.
[35] N.M. Kinnunen, J.T. Hirvi, M. Suvanto, T.A. Pakkanen, Role of the interface between Pd and PdO in methane dissociation, J. Phys. Chem. C 115 (2011) 19197–19202.
[36] S. Gottesfeld, S. Srinivasan, Electrochemical and optical studies of thick oxide layers on iridium and their electrocatalytic activities for the oxygen evolution reaction, J. Electroanal. Chem. 86 (1978) 89–104.
[37] T.C. Wen, C.C. Hu, Hydrogen and oxygen evolutions on Ru-Ir binary oxides, J. Electrochem. Soc. 139 (1992) 2158–2163.
[38] M.V. ten Kortenaar, J.F. Vente, D.J.W. Ijdo, S. Müller, R. Kötz, Oxygen evolution and reduction on iridium oxide compounds, J. Power Sources 56 (1995) 51–60.
[39] S. Trasatti, Electrodes of Conductive Metallic Oxides, Part B, Elsevier Publishing Company, Amsterdam, 1980, pp. 521–626.
[40] R. Mráz, J. Krýsa, Long service life IrO_2/Ta_2O_5 electrodes for electroflotation, J. Appl. Electrochem. 24 (1994) 1262–1266.
[41] W.E. Armstrong, L.B. Ryland, H.H. Voge, US Patent 4, 124 (1978) 538.
[42] M. Sarno, E. Ponticorvo, Continuous flow HER and MOR evaluation of a new Pt/Pd/Co nano electrocatalyst, Appl. Surf. Sci. 459 (2018) 105–113.
[43] R. Vinoth, P. Karthik, C. Muthamizhchelvan, B. Neppolian, M. Ashokkumar, Carrier separation and charge transport characteristics of reduced graphene oxide supported visible-light active photocatalysts, Phys. Chem. Chem. Phys. 18 (2016) 5179–5191.
[44] J. Ohyama, D. Kumadaa, A. Satsuma, Improved hydrogen oxidation reaction under alkaline conditions by ruthenium–iridium alloyed nanoparticles, J. Mater. Chem. A 4 (2016) 15980–15985.
[45] M. Sarno, E. Ponticorvo, D. Scarpa, Ru and Os based new electrode for electrochemical flow supercapacitors, Chem. Eng. J. (2018), https://doi.org/10.1016/j.cej.2018.09.211 In press.
[46] H. Okamoto, The Ir-Ru (iridium-ruthenium) system, J. Phase Equilib. 13 (1992) 565–567.
[47] A.J. Bard, L.R. Faulkner, Electrochemical Methods: Fundamentals and Applications, John Wiley & Sons Inc, New York, 2000.
[48] J.I. Gowda, S.T. Nandibewoor, Electrochemical behavior of paclitaxel and its determination at glassy carbon electrode, Asian J. Pharm. Sci. 9 (2014) 42–49.
[49] M. Hosseini, M.M. Momeni, M. Faraji, Electro-oxidation of hydrazine on gold nanoparticles supported on TiO_2 nanotube matrix as a new high active electrode, J. Mol. Catal. Chem. 335 (2011) 199–204.
[50] M. Srivastava, A.K. Das, P. Khanra, M.E. Uddin, N.H. Kima, J.H. Lee, Characterizations of in situ grown ceria nanoparticles on reduced graphene oxide as a catalyst for the electrooxidation of hydrazine, J. Mater. Chem. A 1 (2013) 9792–9801.
[51] H. Yin, S. Ai, W. Shi, L. Zhu, A novel hydrogen peroxide biosensor based on horseradish peroxidase immobilized on gold nanoparticles–silk fibroin modified glassy carbon electrode and direct electrochemistry of horseradish peroxidase, Sens. Actuator B-Chem. 137 (2009) 747–753.
[52] H. Ma, N. Hu, J. Rusling, Electroactive myoglobin films grown layer-by-layer with poly(styrenesulfonate) on pyrolytic graphite electrodes, Langmuir 16 (2000) 4969–4975.
[53] H.R. Zare, S.H. Hashemi, A. Benvidi, Electrodeposited nano-scale islands of ruthenium oxide as a bifunctional electrocatalyst for simultaneous catalytic oxidation of HY and HA, Anal. Chim. Acta 668 (2010) 182–187.
[54] A. Benvidi, S. Jahanbani, A. Akbari, H.R. Zare, Simultaneous determination of hydrazine and hydroxylamine on a magnetic bar carbon paste electrode modified with reduced graphene oxide/Fe_3O_4 nanoparticles and a heterogeneous mediator, J. Electroanal. Chem. 758 (2015) 68–77.